two near-degenerate orthogonal modes of equal amplitudes and 90° phase difference for CP operation. Also seen in Fig. 1, the single probe feed placed at point A is for achieving left-hand CP operation, while the feed at point B can result in right-hand CP operation.

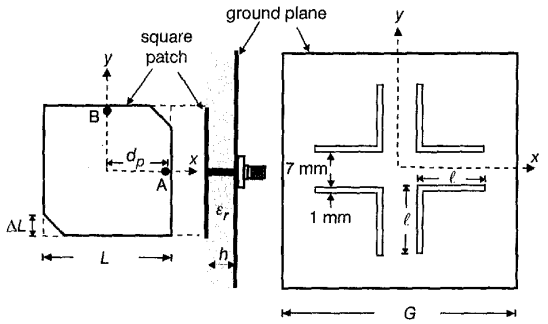

Fig. 1 *Geometry of compact circularly polarised, corner-truncated microstrip antenna with slotted ground plane*

Experimental results and conclusions: Several designs with the feed position at point A for left-hand CP operation were constructed and experimentally studied. Fig. 2 shows the measured return loss against frequency for the cases with $\ell = 0$, 8, 10.5 and 11.5 mm; the case with $\ell = 0$ represents a corresponding regular circularly polarised microstrip antenna with an unslotted ground plane. The corresponding measured data are listed in Table 1 for comparison. The measured results of the axial ratio in broadside direction ($\theta = 0°$) are shown in Fig. 3. From the results obtained, it is clearly seen that the resonant frequency is decreased with increasing slot length. For the case of $\ell = 11.5$ mm, the centre frequency (f_c), defined as the frequency with minimum axial ratio, is only about 74% of that for a corresponding regular CP microstrip antenna (2190 against 2970 MHz). This corresponds to an antenna size reduction of about 45% for the proposed antenna at a fixed operating frequency. It is also noted that the impedance bandwidth and the CP bandwidth, determined from 3 dB axial ratio, of the proposed antenna are increased with the lowering of the centre frequency, which is different from that observed for the compact designs with a slotted radiating patch [1–4]. This characteristic suggests that the embedded slots in the ground plane are more effective than the slots in the radiating patch in lowering the quality factor of the microstrip antenna, and widened CP bandwidth is thus obtained for the proposed design.

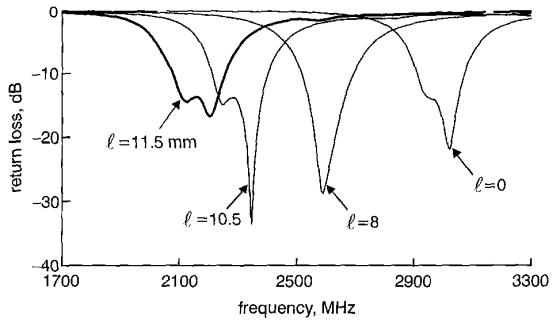

Fig. 2 *Measured return loss against frequency for cases $\ell = 0$, 8, 10.5 and 11.5 mm; $G = 48$ mm, $L = 24$ mm, $h = 1.6$ mm, $\varepsilon_r = 4.4$*

Table 1: CP performances of proposed antenna with slotted ground plane

ℓ	ΔL	d_p	f_c	Impedance BW (10 dB return loss)	CP BW (3 dB axial ratio)	Gain at f_c
(mm)	(mm)	(mm)	MHz	%	%	(dBic)
0	3.5	6.5	2970	5.4	1.4	3.0
8.0	4.0	11.2	2610	6.7	1.7	3.5
10.5	4.0	11.2	2305	8.3	2.0	3.3
11.5	4.0	11.2	2190	8.5	2.1	3.4

$G = 48$ mm, $L = 24$ mm, $h = 1.6$ mm, $\varepsilon_r = 4.4$

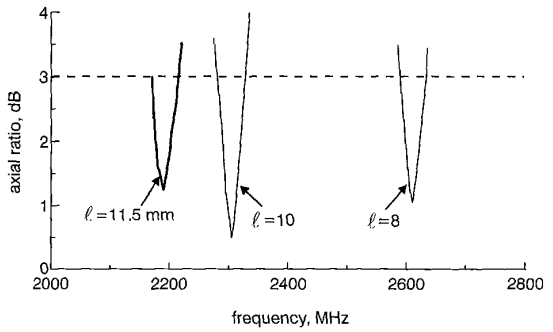

Fig. 3 *Measured axial ratio in broadsight direction for proposed antennas in Fig. 2*

Radiation characteristic of the proposed antenna is also studied. Fig. 4 plots the measured radiation patterns for the case of $\ell = 11.5$ mm at $f = 2190$ MHz; and the measured antenna gain in broadside direction ($\theta = 0°$) is given in Table 1. Good left-hand CP radiation is observed, and the measured antenna gain is ~3.4 dBic, even greater than that (~3.0 dBic) of a corresponding regular circularly polarised microstrip antenna. By using the simulation software IE3D™, the simulated radiation efficiency of the proposed antenna is found to reach ~55%, which is much greater than that (~38%) of a regular circularly polarised micrsotrip antenna with an unslotted ground plane in which the square patch has a side length of 32 mm referenced to the operating frequency at 2190 MHz. The increase in the radiation efficiency may be the reason for the enhanced antenna gain obtained here.

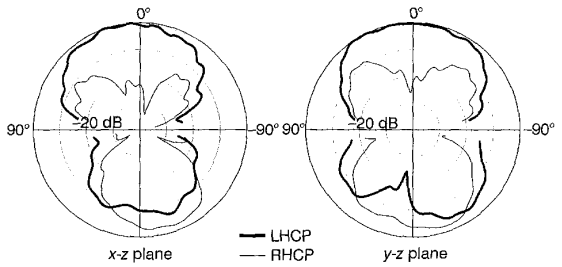

Fig. 4 *Measured radiation patterns in two orthogonal planes for case of $\ell = 11.5$ mm at $f = 2190$ MHz; antenna parameters given in Fig. 2*

15 September 2001
Electronics Letters Online No: 20020425
DOI: 10.1049/el:20020425

H.-D. Chen (*Department of Electronic Engineering, Cheng-Shiu Institute of Technology, Kaohsiung, Taiwan, Republic of China*)

References

1 IWASAKI, H.: 'A circularly polarised small-size microstrip antenna with a cross slot', *IEEE Trans. Antennas Propag.*, 1996, **44**, pp. 1399–1401
2 CHEN, W.S., WU, C.K., and WONG, K.L.: 'Compact circularly polarised microstrip antenna with bent slots', *Electron. Lett.*, 1998, **34**, pp. 1278–1279
3 BOKHARI, S.A., ZURCHER, J.F., MOSIG, J.R., and GARDIOL, F.E.: 'A small microstrip patch antenna with a convenient tuning option', *IEEE Trans. Antennas Propag.*, 1996, **44**, pp. 1521–1528
4 WONG, K.L., and WU, J.Y.: 'Single-feed small circularly polarised square microstrip antenna', *Electron. Lett.*, 1997, **33**, pp. 1833–1834

Interference rejection capabilities of different types of array antennas in cellular systems

S. Durrani and M.E. Bialkowski

The suitable use of array antennas in cellular systems results in improvement in the signal-to-interference ratio (SIR). This property is the basis for introducing smart or adaptive antenna systems. In general, the SIR depends on the array configuration and is a function of the direction of the desired user and interferers. Here, the SIR performance for linear and circular arrays is analysed and compared.

Introduction: An important measure of performance of an array antenna at a base station of a cellular system is its interference rejection or signal-to-interference ratio (SIR) improvement capability. This discrimination ability is in general a function of the number of antenna elements (including their spacing) and the direction of signal arrival of a chosen user and the interferers [1]. It is defined as a reciprocal of the spatial interference suppression coefficient, which is determined as an average cross-correlation between the array steering vector towards a given user and the steering vector towards the interferers. Many research papers have assessed the SIR improvement only for a linear array [1]. However, as this array does not provide uniform coverage in terms of gain or pattern, one may think that such a configuration is not optimal. For example, when a panel positioned on one side of a triangular base station backs this array, its gain degrades in its end-fire directions giving way to interference coming from other directions.

In this Letter we address the problem of selecting optimal array configurations by comparing the SIR improvement ability of two base station antenna systems, one employing a circular array and the other a triangular panel array with a linear array of elements on each side.

Theory: Consider a linear array of N antenna elements receiving signals from M mobile users. The array constitutes one side of a triangular panel array. For simplicity, we consider a uniform linear array (ULA) of omnidirectional antenna elements, spaced a distance $d=\lambda/2$ along the x-axis. Further, we assume that the sources and sensors are located in the xy plane ($\theta=90°$) and that the sources are located in the far field of the array. The direction of arrival (DOA) of sources is then contained in ϕ. The received signal can be expressed as

$$\mathbf{x}(t)=\sum_{k=1}^{M}\mathbf{a}(\phi_k)s_k(t)+\mathbf{n}(t)=\mathbf{A}(\phi_k)\mathbf{s}(t)+\mathbf{n}(t) \tag{1}$$

where $\mathbf{x}(t)$ is $N\times 1$ vector of measured voltages, $\mathbf{s}(t)$ is $M\times 1$ signal vector, $\mathbf{n}(t)$ is $N\times 1$ noise vector and $\mathbf{A}(\phi)$ is $N\times M$ matrix the columns of which are steering vectors of the sources.

The $N\times 1$ steering vector $\mathbf{a}(\phi)$ models the spatial response of the array due to an incident plane wave from the ϕ direction. In general, it is the product of antenna response and the geometrical array factor [2] and is given as

$$\mathbf{a}(\phi_k)=[H_1(\phi_k)\quad H_2(\phi_k)e^{-j\pi\cos\phi_k}\quad H_3(\phi_k)e^{-j2\pi\cos\phi_k}\quad\cdots\quad H_N(\phi_k)e^{-j(N-1)\pi\cos\phi_k}]^T \tag{2}$$

where $H_n(\phi_k)$ denotes the response of antenna element n and $(\cdot)^T$ denotes transpose operation. If mutual coupling between antenna elements is neglected and the individual element patterns are identical, then scaling them with respect to element 1 or absorbing them in $\mathbf{s}(t)$ reduces (2) to

$$\mathbf{a}(\phi_k)=[1\quad e^{-j\pi\cos\phi_k}\quad e^{-j2\pi\cos\phi_k}\quad\cdots\quad e^{-j(N-1)\pi\cos\phi_k}]^T \tag{3}$$

Assuming that user 1 is the desired user, the mean SIR at the array output (SIR_{out}) can be written in terms of input SIR (SIR_{in}) as [1]

$$\mathrm{SIR}_{out}(\phi_1)=\frac{\mathrm{SIR}_{in}}{G_{avg}(\phi_1)} \tag{4}$$

where $G_{avg}(\phi_1)$ is the spatial interference suppression coefficient. Assuming the interferers are uniformly distributed in the range $[0,\ \pi]$, it is given as

$$G_{avg}(\phi_1)=\frac{1}{\pi}\int_0^{\pi}\alpha_k(\phi_1,\phi_k)d\phi_k \tag{5}$$

where $\alpha_k(\phi_1,\phi_k)=(1/N^2)|\mathbf{a}^H(\phi_1)\mathbf{a}(\phi_k)|^2$ and $(\cdot)^H$ denotes Hermitian transpose. Substituting the values from (3), and after some manipulation, we get

$$\alpha_k(\phi_1,\phi_k)=\frac{1}{N^2}\frac{|\sin(0.5*N*\pi(\cos\phi_1-\cos\phi_k))|^2}{|\sin(0.5*\pi(\cos\phi_1-\cos\phi_k))|^2} \tag{6}$$

Next we consider a circular array of N identical omnidirectional antenna elements (such as vertical monopoles) evenly spaced in a circle of radius $R=N\lambda/4\pi$ in the xy plane. This radius is chosen to obtain approximately $\lambda/2$ spacing of the elements, equivalent to that used for the linear array. For plane wave incident in the xy plane, the relative phase at the pth element with respect to the centre of the array is $-(2\pi/\lambda)R\cos(\phi-\Delta\phi)$ where $\Delta\phi=(2\pi p/N)$. The array steering vector can then be written as

$$\mathbf{a}(\phi_k)=[e^{j\pi\cos\phi_k}\quad e^{j\pi\cos(\phi_k-\Delta\phi)}\quad\cdots\quad e^{j\pi\cos(\phi_k-(N-1)\Delta\phi)}]^T \tag{7}$$

Note that similarly as for the linear array this expression neglects mutual coupling effects of the elements of the array. Assuming the interferers are uniformly distributed in the range $[0,\ 2\pi]$, $G_{avg}(\phi_1)$ is given by

$$G_{avg}(\phi_1)=\frac{1}{2\pi}\int_0^{2\pi}\alpha_k(\phi_1,\phi_k)d\phi_k \tag{8}$$

where $\alpha_k(\phi_1,\phi_k)=(1/N^2)|\mathbf{a}^H(\phi_1)\mathbf{a}(\phi_k)|^2$. Substituting the values from (7) and simplifying, we get

$$\alpha_k(\phi_1,\phi_k)=\frac{1}{N^2}\left|\sum_{p=1}^{N}\exp[j\pi(\cos(\phi_k-(p-1)\Delta\phi)-\cos(\phi_1-(p-1)\Delta\phi))]\right|^2 \tag{9}$$

Results: Fig. 1 shows a plot of the spatial interference suppression coefficient $G_{avg}(\phi_1)$ for a linear array for different numbers of elements N. The curves are U-shaped, with a broad minimum, implying that interference reduction is maximum over a certain range of ϕ_1, centred at $\phi_1=90°$ (broadside). However, the exact amount of SIR at the array output is dependent on ϕ_1. The presented result confirms our earlier expectation that for a linear array its discrimination against interferers (in terms of SIR) is best in the broadside direction of the array and deteriorates in its end-fire directions.

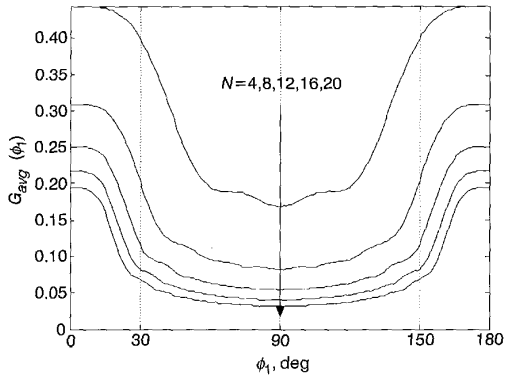

Fig. 1 *Variation of spatial interference suppression coefficient ($G_{avg}(\phi_1)$) with ϕ_1 for linear array*

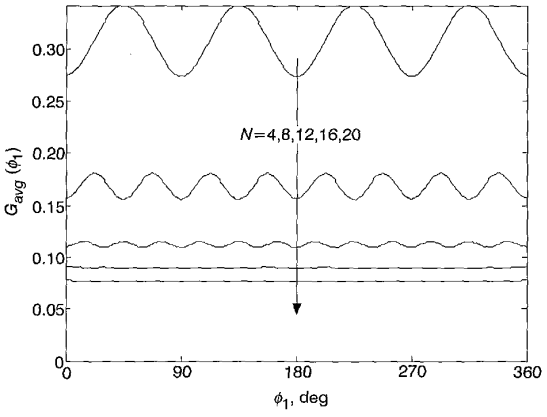

Fig. 2 *Variation of spatial interference suppression coefficient ($G_{avg}(\phi_1)$) with ϕ_1 for circular array*

The plot of $G_{avg}(\phi_1)$ for a circular array is shown in Fig. 2. For a small number of antenna elements, the SIR improvement shows an oscillatory variation. However, as N increases, the curves flatten, indicating uniform SIR improvement over all angles.

Table 1 shows the variation of mean of $G_{avg}(\phi_1)$ over ϕ_1 (an average of $G_{avg}(\phi_1)$ over the assumed range of ϕ_1) for different N for linear and circular arrays. The values reveal that for large N, the interference reduction capability reaches an asymptotic level, implying onset of diminishing returns. Also, for the same values of N, linear and circular geometries have nearly the same mean of $G_{avg}(\phi_1)$ over ϕ_1. However, it must be noted that for the same N, the triangular panel array would require employing three times the total number of antenna elements to obtain comparable performance to a circular array.

Table 1: Mean of $G_{avg}(\phi_1)$ over ϕ_1 for linear and circular arrays

N	Average of $G_{avg}(\phi_1)$ over ϕ_1	
	Linear array	Circular array
4	0.3029	0.3089
6	0.2143	0.1973
12	0.1184	0.1124
24	0.0652	0.0640
36	0.0459	0.0457
48	0.0357	0.0354
60	0.0294	0.0287
72	0.0251	0.0242

Conclusions: We have provided and compared analytical results for the average SIR improvement for linear and circular arrays employed at a base station of a cellular system. It is shown that for a full angular range surrounding a base station, a circular array provides a more uniform improvement in terms of SIR than a linear array. This finding indicates the need and importance of investigating circular or conformal antenna systems [3] that feature a broad angular view. Such arrays may offer better SIR performance than linear arrays, as well as the additional advantage of less severe mutual coupling effects due to the array curvature.

Acknowledgments: The PhD research of S. Durrani is supported by an International Postgraduate Research Scholarship.

1 February 2002
Electronics Letters Online No: 20020439
DOI: 10.1049/el:20020439

S. Durrani and M.E. Bialkowski (*School of Information Technology & Electrical Engineering, The University of Queensland, Brisbane, QLD 4072, Australia*)

E-mail: dsalman@itee.uq.edu.au

References

1 SONG, Y.S., and KWON, H.M.: 'Analysis of a simple smart antenna for CDMA wireless communications'. IEEE Vehicular Technology Conf., Houston, TX, USA, May 1999, pp. 254–258
2 GODARA, L.C. (Ed.): 'Handbook of antennas in wireless communications' (CRC Press, 2002), Chap. 20
3 KABACIK, P., and BIALKOWSKI, M.E.: 'Cylindrical array antennas and their applications in wireless communications systems'. Proc. 16th Int. Conf. on Applied Electromagnetics and Communications, Dubrovnik, Croatia, October 2001

Microstrip-fed dual-frequency printed triangular monopole

H.-M. Chen

A new, compact, microstrip-fed printed equilateral triangular monopole with dual-frequency operation is described. Various frequency ratios, within the range 1.37–1.75, of the two operating frequencies can be obtained by varying the trapezoidal slit dimensions of the triangular patch. Omnidirectional radiation patterns of the two operating frequencies are given for the proposed antenna.

Introduction: The rapid developments in the wireless communications industry demand novel designs that can be used in more than one frequency band and in size reduction. The standard monopole is probably the most widely used antenna on existing mobile telecommunication applications. To meet the requirements for modern mobile applications, some printed triangular monopole antennas [1, 2] with reduced size and broadband operation are reported. For such printed triangular monopoles, the antenna length is reduced to about 0.6 times that of a simple strip monopole. Recently, dual-frequency monopole antennas were developed and investigated for cellular applications [3, 4]. The antenna in [3] consists of a straight radiating element and a helically wound element, and the straight radiating element acts as the antenna radiator. The electrical length of the antenna is usually between three-eighths of the wavelength and half of the wavelength. The antenna in [4] uses one monopole with two equal length branches. The length of the monopole is approximately one-quarter of a wavelength at the centre frequency of the low band.

Presented in this Letter is a new microstrip-fed dual-frequency printed triangular monopole antenna, which can be used in one radiating element and in tunable frequency ratio. Furthermore, due to the increased effective current patch in the triangular monopole, compared with a simple strip monopole of the same length, the required monopole length at a fixed operating frequency can be reduced, i.e. the electrical length of the proposed antenna is less than one-quarter of a wavelength.

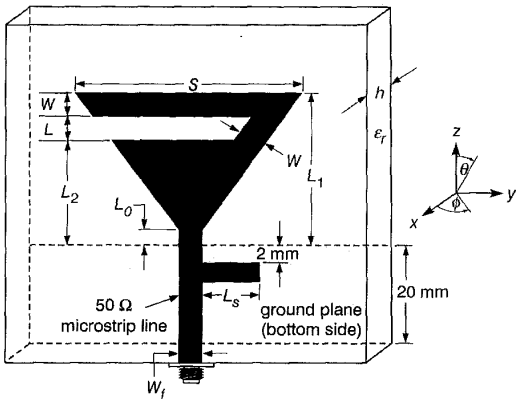

Fig. 1 *Geometry of microstrip-fed printed triangular monopole*

Antenna configuration: Fig. 1 shows the geometry of a printed equilateral triangular monopole of width S and length L_1. The triangular monopole is printed on an FR4 substrate of thickness h and relative permittivity ε_r. The trapezoidal slit with vertical height of L is etched on the equilateral triangular patch. The location of the slit with respect to the sides of the triangular patch is denoted as W, i.e. in the present design, the length of the lower triangular patch has the relation $L_2 = L_1 - L - W$. A 50 Ω microstrip line with an open-circuited tuning is used for feeding the proposed antenna at the apex angle of the equilateral triangular patch. The truncated ground plane on the backside of the substrate is used as a reflector element. The tuning stub has a length of L_s and a gap distance from the edge of the truncated ground plane is chosen as 2 mm. The section of the tuning stub has a width of W_f, the same as the width of the microstrip line. The distance between the end of the monopole and the terminal of the microstrip line is denoted as L_0 ($=(W_f/2)\tan 60°$). The tuning stub length (L_s) was found to be very effective in controlling the coupling of the electromagnetic energy from the microstrip feed line to the triangular monopole, and good impedance matching for the dual-band antenna can be achieved

Experimental results and discussion: Typical proposed antenna were implemented and tried. Fig. 2 shows the measured return loss for the proposed antenna with various slit height (L), as the triangular monopole length (L_1) and the strip width (W) are fixed. First, note that only the fundamental mode is excited for the antenna A, i.e. antenna A is a simple triangular monopole without a slit ($L = 0$ mm). However, when the slit etched on the triangular patch is present, a new resonant frequency can be excited. The corresponding dual-frequency